OPEN ACCESS

ACTA METALLURGICA SLOVACA

2026, VOL. 32, NO. 3, 190-198

RESEARCH PAPER

Probabilistic modeling and industrial validation of ore grinding in drum mills using a physically motivated activation factor

Gulnara Katkeeva[1], Astra Makasheva[1,2], Vitaliy Malyshev[1], Natalya Lu[1], Gulnazira Shaikhova[2], Armat Zhakan [1]*

[1] Zh. Abishev Chemical and Metallurgical Institute, Yermekov street 63, 100009, Karaganda, Kazakhstan
[2] Abylkas Saginov Karaganda Technical University, Ave. Nursultan Nazarbayev, 56, 100026, Karaganda, Kazakhstan

*Corresponding author: s.shaikhova@ktu.edu.kz / Abylkas Saginov Karaganda Technical University, Ave. Nursultan Nazarbayev, 56, 100026, Karaganda, Kazakhstan

Received: 10.06.2026
Accepted: 15.08.2026

ABSTRACT

This study presents a modified activation factor for probabilistic ore-grinding models in drum mills, based on thermodynamic considerations. The proposed formulation accounts for the combined contribution of the potential and kinetic energies of grinding bodies and refines the effective ball fall height in the cascading mode from 0.5D to 0.83D, resulting in a 17.6% increase in the estimated mechanical energy transfer. The activation energy is estimated from the material melting temperature, providing an alternative to conventional empirical fitting coefficients. The model was evaluated using quartz grinding calculations and industrial data from an MShR 3.2 × 3.1 mill at the Zhezkazgan concentrator. The comparison between the calculated and experimental particle size distributions showed a statistically significant correlation (R = 0.628), indicating that the proposed approach provides a physically meaningful description of the grinding process under the investigated industrial conditions.

Keywords: grinding; drum mill; activation factor; comminution; mechanical energy; probabilistic model.

INTRODUCTION

Grinding is a complex, energy-intensive, and cost-demanding process. Adequate comminution of ore materials promotes more efficient, selective, and rapid physicochemical transformations, particularly flotation reactions, while also enhancing the efficiency of downstream metallurgical processes such as drying and roasting.

Extensive research has been conducted on the mechanisms of mineral particle breakage [1–3], the analysis of raw material processing and grinding efficiency in various types of mills [4–6], the development of mathematical models and methods for comminution [7–9], the identification of process patterns under automated control [10–12], and the investigation of ore grinding kinetics in different types of equipment [13–14].

Previous studies [15–17] have examined the influence of the physicochemical properties of ores and grinding conditions on product quality and equipment wear. For example, in the work [15] demonstrated that the moisture content of raw copper ore and particle classification significantly affect grinding efficiency. Based on these parameters, the authors established optimal drying conditions, enabling the automation of the grinding process control system. In the work [16], the influence of various operating parameters of a ball mill and hydrocyclone on the development of an ideal mixing model for copper ore was investigated. The authors of in the work [17] emphasized the importance of selecting appropriate grinding equipment by comparing conventional and high-pressure grinding rolls using iron ore as a representative material.

Studies [18–20] focused on the modeling and optimization of grinding processes, particularly considering particle size distribution and operating parameters. The primary objective of these investigations was to improve grinding efficiency while reducing energy consumption. For instance, in the work [20] proposed a unified approach in which the grinding behavior of different ore types is represented by a single parameter—the time required to achieve the target mean particle size. Incorporating this parameter significantly improved the accuracy of predictions of product quality in industrial grinding mills.

Other researchers [21–23] have concentrated on adapting processing equipment to the specific characteristics of different ores, including uranium and platinum ores. Studies of particle morphology are presented in the works [24–25], whereas the grinding kinetics of various ore types have been examined in the works [26–27].

A review of the published literature indicates that achieving a comprehensive understanding of the grinding process remains challenging because of its inherently probabilistic nature. This often leads to operational inaccuracies that adversely affect subsequent flotation performance, reducing the recovery of valuable non-ferrous metals into concentrates and impairing subsequent smelting and refining operations. These shortcomings are reflected in excessive electricity consumption during ore grinding. Although the theoretical energy efficiency of the grinding process is approximately 13.4%, its practical efficiency rarely exceeds 10%. Consequently, approximately 3.4% of the energy losses can be attributed to deviations from optimal operating conditions caused by subjective factors, particularly the insufficient characterization and understanding of the grinding mechanism.

Therefore, the development of unified mathematical models that accurately describe ore grinding processes remains an important and timely research objective.

The authors of [28] developed a probabilistic model describing the grinding of ore in ball mills. The model accounts for the influence of several factors on the grinding rate of ore particle fractions with an average diameter of d_j. The collisions between grinding media and ore particles in rotating mills were treated analogously to the collision kinetics of bimolecular reactions, where the reaction rate of components A and B is represented through the interactions between ore particles and grinding balls (τ denotes the process duration). The general probabilistic form of the grinding model is expressed as follows:

$$P_n = P_{fr} P_a P_{st} P_{conc} P_j \quad (1.)$$

where P_n is the probability of formation of the n-th particle size fraction; P_{fr} is the frequency factor; P_a is the activation factor; P_{st} is the steric factor; P_{conc} is the concentration factor; and P_j is the volumetric fraction of the total mass of unbroken ore particles available for contact with the grinding media.

The rate of the mechanical reaction described by Eq. (1) can be expressed as follows:

$$v = -\frac{\partial P_j}{\partial \tau} = P_{fr} P_a P_{st} P_{conc} P_j, \mathrm{s}^{-1} \quad (2.)$$

This analogy is based on the fact that the rate equation is mathematically a universal expression describing the probability of a sequence of simultaneous and consecutive events. These include the simultaneous presence of an ore particle and a grinding ball within a given volume element, represented by the product P_j, P_{conc}; the collision of a grinding ball with an ore particle, taking into account their different sizes and the formation of "dead zones" (the steric factor); and the fracture of the ore particle upon impact (the activation factor). These events occur at a frequency determined by the mill's rotational speed when operating in the cascading regime.

After substituting all contributing factors, the expanded form of the model is expressed as follows:

$$-\frac{\partial P_j}{\partial \tau} = \frac{8d_j(d_b - d_j)\omega G_b G_g P_j}{d_b^2\left(1 + 2\omega\sqrt{2D/g}\right)\left(G_b/\gamma_b + G_g/\gamma_g\right)^2 \gamma_b \gamma_g} exp\left(-\frac{E_a}{RT + \frac{3MmgD}{\pi d_j^3 \gamma_g}}\right) \quad (3.)$$

where d_b is the diameter of the grinding balls (m); d_g is the diameter of the ore particles (m); G_b is the mass of the grinding balls in the mill (kg); γ_b is the density of the ball material (kg/m^3); G_g is the mass of the ore being ground (kg); γ_g is the density of the ore particles (kg/m^3); ω is the rotational frequency of the mill operating in the cascading regime (s^{-1}); D is the internal diameter of the mill (m); g is the acceleration due to gravity (m/s^2); E_a is the activation energy of the material (J/mol); M is the molar mass of the material (kg/mol); m is the mass of the grinding balls (kg); R is the universal gas constant (8.31441 J/(mol·K)); and T is the absolute temperature (K).

As can be seen from Eq. (3), only P_j is time-dependent. Therefore, all remaining parameters can be combined into a single constant representing the particle breakage rate (s^{-1}).

$$k_j = -\frac{\partial P_j}{\partial \tau} = \frac{8d_j(d_b - d_j)\omega G_b G_g}{d_b^2\left(1 + 2\omega\sqrt{2D/g}\right)\left(G_b/\gamma_b + G_g/\gamma_g\right)^2 \gamma_b \gamma_g} exp\left(-\frac{E_a}{RT + \frac{3MmgD}{\pi d_j^3 \gamma_g}}\right) \quad (4.)$$

Accordingly, Eq. (3) can be rewritten as:

$$v = -\frac{\partial P_j}{\partial \tau} = k_j P_j, \mathrm{s}^{-1} \quad (5.)$$

The particle breakage rate constant incorporates all the principal process parameters, including the average particle size of the j-th size fraction, the diameter and density of the grinding balls, the mass and density of water in the mill, the mass and density of the ball charge, the mass of ore in the mill, the mill rotational speed, the internal mill diameter, the energy barrier for particle fracture, and the molar mass of the material being ground. The determination of the particle breakage rate constant, k_j, reported in the work [28], made it possible to establish a direct relationship describing the content (yield) of any size fraction, P_n, at any grinding time, τ accounting for both the breakage of coarser particles and the accumulation of finer fractions:

$$P_n = P_{0n}e^{-k_n\tau} + \sum_{j=1}^{n-1} P_{0j}\left(\prod_{i=j}^{n-1} k_i\right)\sum_{m=j}^{n}\frac{e^{-k_m\tau}}{\prod_{\substack{i=1\\ i\neq m}}^{n}(k_i - k_m)} \quad (6.)$$

Where P_{0j} is the initial particle size distribution of the ore (dimensionless); n is the index of the calculated size fraction; j denotes the indices of the preceding size fractions and the corresponding grinding stages; and $m=j$ represents the transition operation from one structural component to another. The equation also includes empirical constants that account for the agglomeration of fine particles within the compressed particle bed prior to impact, as well as the mechanical strength of the ore. In combination with the grinding time, τ (s), and the exponential terms, the resulting fraction content is dimensionless.

The objective of this study is to determine the activation factor in the probabilistic model of ore grinding in order to adapt it to the operating conditions of industrial grinding mills.

MATERIAL AND METHODS

The foundational formula for the activation factor

$$P_a = exp\left(-\frac{E_a}{RT + E_{mec}}\right) \quad (7.)$$

The approach adopted in this study, based on the derivation of the Boltzmann distribution by incorporating the contribution of mechanical energy, provides an opportunity to refine the expressions for both the activation energy and the mechanical energy. The activation energy for grinding was estimated from the material's heat of fusion and, as a first approximation, was assumed to be equal to the heat of fusion of quartz, the principal rock-forming mineral and the hardest component of the ore. The mechanical impact energy was taken to be equal to the potential energy of the grinding ball converted into impact energy, mgh, where the average falling height was estimated as $h \sim 0.5D$, as reflected in the following equation:

$$P_a = exp\left(-\frac{Ea}{RT + 0{,}5MgD(b/\gamma_{gr})(d_b/d_j)}\right) \quad (8.)$$

These approximations made it possible to reveal the principal qualitative features of the highly complex grinding process. However, in some cases, the probabilistic model required correction through an adaptation coefficient for the grinding rate constant to improve agreement with experimental data. Such a correction may result from inaccuracies in estimating one or more of the fifteen parameters included in the probabilistic model. At the same time, the model itself remains open to further refinement through a more rigorous interpretation of each probabilistic factor, particularly the activation factor [29].

Activation energy is a fundamental concept applicable to all energy-driven processes, including mechanical processes, between which equivalent energy transformations can occur.

The activation energy for grinding may be estimated from the heat of fusion of the ore; however, this approach requires dedicated experimental measurements. A more practical approach is to estimate the activation energy from the additional thermal energy acquired by the material when it is heated from the initial temperature, RT, to the melting point, RT_m which can be expressed as follows:

$$E_a = RT_m - RT = R(T_m - T) \quad (9.)$$

As demonstrated in the work [30] for estimating the useful energy associated with plastic deformation, this approach requires only the melting temperature of the material, which is well established for various ores and governs the thermal conditions of pyrometallurgical processes.

The resulting expression differs fundamentally from the conventional formulation. In the proposed model, the mechanical energy is not subtracted from the activation energy in the numerator, which may otherwise lead to physically unrealistic results (e.g., $P_p > 1$ when $E_{mec} > E_a$). Instead, the mechanical energy is added to the thermal energy in the denominator, thereby ensuring that the probability of particle fracture remains within mathematically and physically valid limits.

For the grinding process considered in this study, the thermal barrier associated with the melting temperature, RT_m, has been adopted. However, the investigated approaches produced only minor differences in the calculated results. This may be attributed to the melting barrier being significantly removed from the actual operating conditions of grinding. In practice, the objective is not to activate melting or excessive softening of the material but rather to activate its fracture.

The present study addresses this issue using a generalized probabilistic approach to the interpretation of fracture and activation phenomena in chemical, physical, and mechanical processes. Meanwhile, the widely used Frenkel equation, based on the hole theory of liquids, appears to be inconsistent with the probabilistic interpretation because the dynamic viscosity, η is related to the activation energy of viscous flow only through a pre-exponential factor having the dimensions of specific thermal energy:

$$\eta = Ae^{\frac{U}{RT}} \quad (10.)$$

where A was the pre-exponential factor with the dimensionality of viscosity. However, it was difficult to reconcile this with viscosity in terms of meaning. As $T \to \infty$, $\eta \to A$, and as $T \to 0$, $\eta \to \infty$. Therefore, this equation was recommended for use only within narrow temperature intervals, where $A \approx$ const. However, the equation acquires a physically consistent interpretation after applying an equivalent transformation by taking the reciprocal of both sides of the equation, as proposed in Ref. [29].

$$1/\eta = 1/A\ exp(-vU/RT) \quad (11.)$$

The reciprocal of viscosity is, by definition, fluidity. Consequently, U acquires the physical meaning of the activation energy of fluidity, which can be promoted by increasing the probability of particle breakage. This interpretation is consistent with the forward direction of the process and provides agreement between Eqs. (11) and (7), unlike the conventional interpretation based on the activation energy of viscosity.

Within the probabilistic multifactor model described by Eq. (1), it is essential to preserve the direct probabilistic interpretation of each contributing factor: the concentration factor, P_{conc}, representing the probability of particle presence within the interaction zone; the steric factor, P_{st}, representing the probability of collisions; the activation factor, P_a, representing the probability of particle

fracture; and the frequency factor, P_{fr}, representing the probability of maintaining the cascading operating regime of the mill.

As for the main object of our study, the use of the well-known Bochvar-Tammann optimal plasticity temperature proved to be successful:

$$T_{pl} = 0.5T_m \quad (12.)$$

This temperature was repeatedly confirmed by experiments and practical data [28].

We were able to find an earlier analytical justification based on the Boltzmann distribution and the concept of chaoticized particles [30]. This justification was grounded in the temperature dependence for liquid-like particles. The proportion of these particles increased with the destruction of the substance and even coincided with the inflection point temperature of the Bochvar-Tammann temperature, $T_m/2$ or $0.5T_m$.

As is well known, particle fracture is initiated by plastic deformation, while the optimum range of plasticity is determined by the Bochvar–Tammann temperature. Since this temperature can be determined analytically, it improves the prediction of particle size distribution during the initial stage of the grinding process.

However, because the structural changes occur in a solid material, a more appropriate temperature dependence is that based on the fraction of crystal-mobile particles. This function possesses an inflection point corresponding to the maximum gradient of activation, which governs the onset of classical plastic deformation leading to particle fracture. The position of this inflection point is determined by successive differentiation of the equation describing the fraction of crystal-mobile particles:

$$P_{crm} = 1 - exp\left(-\frac{Tm}{T}\right) = 1 - exp(T_m T^{-1}) \quad (13.)$$

Omitting the intermediate mathematical derivations, the resulting equation describing both the lower and upper boundaries of the effective plasticity range can be written as follows:

$$T_{1,2} = \frac{\left(3 \pm \sqrt{3}\right) \triangle H_m}{6R} \cong (0{,}23 \div 0{,}82)T_m \quad (14.)$$

As is well known, the destruction of various materials began with plastic deformation [30], and this fully applied to the grinding process, as evidenced by the external appearance of mill spare waste (“scats”).

The relationship between the height of the falling ball and the internal diameter of the mill required correction. A more rigorous justification was provided by considering the well-known filling degree (working volume) of the mill. According to [13], this ranged from 30-50% of the total volume. For calculation purposes, the average value of 40% was assumed. In this case, for the cascading mode, one considered the scenario where this volume, in the form of a hollow cylinder, adjoined the inner surface of the drum. It was reduced to the area of a ring that occupied 40% of the area of the circle (**Fig. 1**). The internal diameter of the ring d was determined using the following relations:

$$d = \frac{\pi D^2}{4} - 0.4\frac{\pi D^2}{4} = 0.6\frac{\pi D^2}{4} \quad (15.)$$

From this,

$$d = D\sqrt{0{,}6} \approx 0.775D \quad (16.)$$

Alternatively, for the general expression describing the mill filling ratio (V_{work} is the working volume and V_{gen} is the total mill volume), the equation can be written as follows:

$$d = D\sqrt{1 - \frac{V_{work}}{V_{gen}}}$$

The geometry of the cascading part of the ring followed a parabolic trajectory. However, for the calculation of the potential energy of the ball, only the height difference between the release and impact points was required. This height difference, based on geometric considerations, was approximated (Figure 1) as:

$$h \cong \frac{D+d}{4} + d/2 = \frac{D+3d}{4} = \frac{D+3D\sqrt{0{,}6}}{4} = \frac{D\left(1+3\sqrt{0{,}6}\right)}{4} = 0.83D \quad (17.)$$

This value substantially exceeded (by a factor of 1.66) the previously accepted approximation $h = 0.5D$.

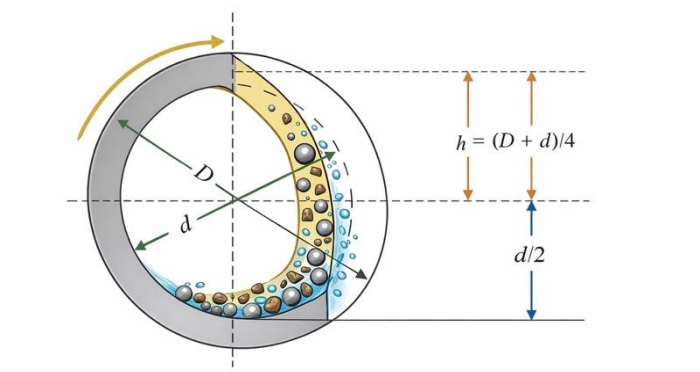


Fig. 1 Schematic of the motion of the mixture of balls, ore and water in the waterfall regime at a mill filling degree (working volume) of 40 %.

The same schematic was used to account for the kinetic energy of the ball at the point of detachment from the inner surface of the drum. This energy remained as the horizontal component of the force, velocity, and energy vectors.

This component was estimated based on the average circumferential velocity of the mixture, which was calculated from its average diameter, given by:

$$D_{average} = \frac{D+d}{2} = \frac{D+D\sqrt{0{,}6}}{2} = D\left(\frac{1+\sqrt{0{,}6}}{2}\right) = 0.887D \quad (18.)$$

Substituting this value into the formula for the circumferential velocity, we obtained:

$$V = \pi D_{sr}\omega = 2.79D\omega \quad (19.)$$

With this, the kinetic energy of the ball was found as:

$$E_{kin} = m_b V^2/2 = 3.885 m_b D^2 \omega^2 \quad (20.)$$

Since the angular velocity in the cascading mode of rotation was related to the mill diameter as:

$$\omega = 0.5762/\sqrt{D} \quad (21.)$$

the final expression took the form:

$$E_{kin} = 1.29 m_b D \quad (22.)$$

From the comparison with the potential energy of the ball (after substituting h = 0.83D)

$$E_{pot} = mgh = 0.83 m_b g D \quad (23.)$$

it followed that the ratio:

$$\frac{E_{pot}}{E_{kin}} = \frac{0.83 m_b g D}{1.29 m_b D} = 5.67 \quad (24.)$$

for the cascading rotation mode remained constant. This was in full accordance with the consideration of the critical angular velocity for the onset of centrifugation:

$$\omega_{cr} = \frac{1}{\pi}\sqrt{\frac{g}{2D}} = \frac{0.705}{\sqrt{D}} \quad (25.)$$

From this point, the angular velocity of the cascading mode was taken in a specific decreasing proportion, as shown in equation (20).

The ratio (24) established that the potential energy of the ball at the point of detachment significantly exceeded the kinetic energy of rotation, comprising 85% of their total sum. Their combined effect was expressed through a correction factor to the potential energy:

$$E_{mec} = E_{pot} + E_{kin} = E_{pot} + 0.176E_{pot} = 1.176\ E_{pot} \quad (26.)$$

To clarify the physical interpretation of the proposed model and the sequence of energy transformations during grinding, a schematic representation is provided (**Fig. 2**).

The **Fig. 2** illustrates the relationship between the motion of grinding bodies and the resulting particle breakage through successive energy transformations. The total mechanical energy is formed by combining potential and kinetic energy contributions and is further used in the probabilistic description of the activation factor. This representation highlights the physical basis of the modified model and its connection to the grinding process.

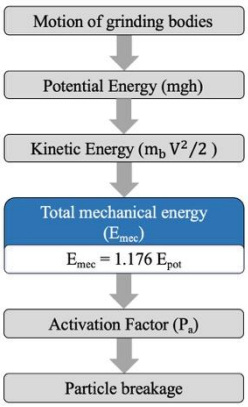


Fig. 2 Schematic representation of energy transformation from grinding body motion to particle breakage in a drum mill.

Thus, taking into account equation (23) for $E_{pot,}$ the total mechanical energy was found to be:

$$E_{mec} = 0.976 m_b g D \approx m_b g D$$

In other words, the loss of the calculated potential energy during rotation due to the reduction in the fall height from $h = D$ to $h = 0.83D$ was compensated by the acquired kinetic energy at the point of detachment from the inner surface of the drum.

Thus, the general expression for the activation factor (7):

$$P_a = exp\left(-\frac{\Delta H_m}{RT + E_{mec}}\right)$$

was presented in the following modified forms, with the mass of balls and grains converted into their sizes (diameters) through the corresponding densities.

The original model, with activation energy equal to the heat of fusion and the previously accepted average fall height of the ball $h = 0.5D$, was expressed as:

$$P_a = exp\left(-\frac{\Delta H_m}{RT + 0{,}5MgD(\gamma_b/\gamma_{gr})(d_b/d_j)^3}\right) \quad (27.)$$

The same model, but accounting for $E_{mec} \cong m_b gD$, was written as:

$$P_a = exp\left(-\frac{\Delta H_m}{RT + MgD(\gamma_b/\gamma_{gr})(d_b/d_j)^3}\right) \quad (28.)$$

A model was proposed with activation energy for the thermal motion of particles, inversely proportional to the heating of the substance, with activation being zeroed at the thermal barrier variant, and $E_{mec} \approx m_b gD$:

$$P_a = exp\left(-\frac{R(T_t - T)}{RT + MgD(\gamma_b/\gamma_{gr})(d_b/d_j)^3}\right) \quad (29.)$$

Measurements were conducted at the Zhezkazgan concentrator. The feed comprised a blend of hard mine ore and up to 40-45% ore from the Zhomart deposit, whose hardness is comparable to that of Zhezkazgan ores. A grate-discharge mill MShR 3.2 × 3.1 operates at the first stage of grinding in a closed circuit with a spiral classifier (KSN).

Measurement results:

The internal mill diameter (with liners) is 3.0 m.

The mill length is 3.1 m.

The ball charge occupies 37.4% of the mill volume.

The mass of grinding media in the mill is 37800 kg.

The bulk density of the balls is 4600 kg/m^3.

Ball size distribution: 100 mm – 48%, 80 mm – 17%, 60 mm – 28%, pebbles (~30 mm) – 7%.

Throughput (Q, on a dry basis): ore – 64.75 t/h; sands – 9 t/h; mill discharge – 73.75 t/h.

Moisture content: ore – 1.9%; sands – 8.3%; discharge – 24.2%.

Density of the balls is 7860 kg/m^3; ore density is 2700 kg/m^3.

The mill is filled with pulp (a mixture of ore, sands, and water) up to the "mirror" level, i.e., directly above the ball charge, occupying the voids within the bulk of the grinding media.

The mill rotational speed in cascading mode is 18.2 rpm.

RESULTS AND DISCUSSION

To illustrate, an example was provided using these three probability models for the destruction of quartz ore in a mill with an internal diameter of 3 meters (including the lining) at a temperature of 298 K. Steel balls with a diameter of d_b = 0.06 m and a density ofγ_b = 7860 kg/m^3 were used. The reference data for quartz included: molecular weight M = 0.0601 kg/mol, density γ_{gr} = 2700 kg/m^3, melting heat ΔH_m = 9170 J/mol, and melting point T_m = 1883 K.

After substituting these values, along with the gas constant R = 8.31441 J/(mol·K), into formulas (27)-(29), the following calculated variants were obtained:

$$P_a(27) = exp\left(-\frac{9170}{2478 + 5.560 \cdot 10^{-4} d_j^{-3}}\right)$$

$$P_a(28) = exp\left(-\frac{9170}{2478 + 1.112 \cdot 10^{-3} d_j^{-3}}\right)$$

$$P_a(29) = exp\left(-\frac{13178}{2478 + 1.112 \cdot 10^{-3} d_j^{-3}}\right)$$

In this case, the Bochvar-Tammann temperature was taken into account similarly to models (27)-(29). It was most closely aligned with model (27), where instead of T_m, half of the barrier height $0.5T_m$ was used in the numerator:

$$P_a = exp\left(-\frac{R(0{,}5T_m - T)}{RT + MgD(\gamma_b/\gamma_g)(d_b/d_j)^3}\right) \quad (30.)$$

In the calculated variant, under the previously mentioned external conditions, the following expression was obtained:

$$P_a(30) = exp\left(-\frac{8.31441(0.5 \cdot 1883 - 298)}{2478 + 1.112 \cdot 10^{-3} d_j^{-3}}\right) = exp\left(-\frac{5350}{2478 + 1.112 \cdot 10^{-3} d_j^{-3}}\right)$$

The calculation results, starting with a grain diameter of d_1 = 0.01 m and successively halving the grain size, were provided in the **Table 1** and **Fig. 3**.

Table 1 Dependence of the activation factor (destruction probability) in models P_a (27), P_a (28), P_a (29), and P_a (30) on the size of the ground grains, applied to industrial conditions for d_b = 0.06 m and D = 3 m.

j	dj, m	Pa (27)	Pa (28)	Pa (29)	Pa (30)
1	0.010	0.049	0.078	0.026	0.225
2	0.005	0.266	0.447	0.314	0.625
3	2.5·10-3	0.786	0.883	0.836	0.930
4	1.05·10-3	0.981	0.991	0.986	0.994
5	6.25·10-4	0.996	0.998	0.997	0.999
6	3.125·10-4	1.000	1.000	1.000	1.000

Among the proposed models, Eqs. (27) and (29) are considered the most suitable, as they employ the heat of fusion and the activation energy, expressed as $R(T_m\text{-}T)$ as the thermal barriers. Furthermore, as shown in Figure 5, the close agreement between the results obtained from these two equations enables a direct comparison of the alternative approaches based on the heat of fusion, ΔH_m , and the activation energy, E_a.

The strong similarity of the corresponding curves indicates the existence of a functional relationship between these two energy quantities and highlights the need for a more comprehensive investigation of their underlying physical connection.

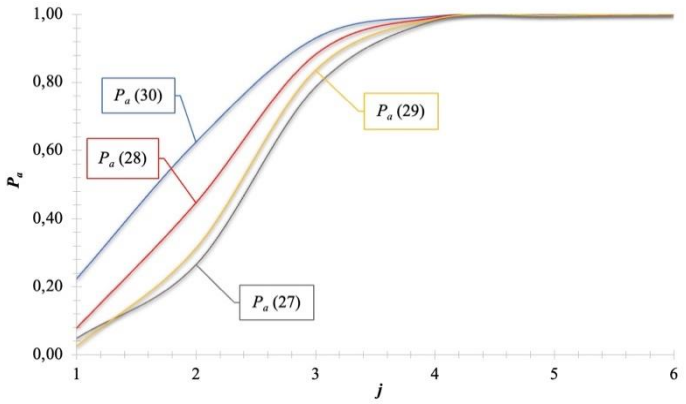


Fig. 3 Dependence of the grain destruction probability on their size according to models P_a (27) - P_a (30).

As for the use of the Bochvar-Tammann temperature as the activation energy barrier for grinding, this barrier proved to be particularly suitable. This was due to the alignment of both physical and mathematical reasoning. The inflection point of the primary temperature dependence strictly represented the region where the gradient of the function changes with respect to the argument. The maximum corresponded to the second derivative, which was the rate of change.

Thus, the activation barrier ceased to be an arbitrary kinetic argument. It became a reference value. It should decrease as it approached both the right and left asymptotes. This behavior was reflected in the activation barrier formula:

$$E_a = R(0{,}5\,T_m - T)$$

Here, the value of E_a was found at $T=0{,}5T_m$.

A similar effect was achieved due to the additional energy in our case. The effective fall height of the balls in the mill was increased by a factor of two, from *0.5D to 0.83D.* In this case, the direct action of the fall height factor was implemented.

Returning to the calculation of the structures of heterogeneous ore, activation energy and the Bochvar-Tammann temperature were used, based on data from **Table 2** and **Fig. 3**. These data, along with the sharp improvement in grinding efficiency, were noted. The efficiency improved especially for steep ascension, by more than an order of magnitude. At the melting temperature of quartz, 1833 K, the activation thermal barrier was half of this value, or 942 K (668 °C, red heat temperature). The beginning of the optimal melting range corresponded to a value of $0.23T_m$ = 433 K = 160 °C. This temperature was technically quite accessible.

The data indicated that the additional consideration of the kinetic energy of the ball in model P_a (28) significantly enhanced the destructibility of the grains (R = 0.973, t_R = 74 > 2). On the other hand, using $R(T_m–T)$ as the activation energy for destruction in model P_a (29) yielded comparable results to the previously accepted energy barrier in model P_a (27) (R = 0.996, t_R = 520 >> 2). This justified the possibility of a more accessible estimation of activation energy through the material's melting temperature.

A notable result is the close agreement between the model predictions across different formulations. This included a practical coincidence at the point where the curve transitioned into the horizontal asymptote as $T \to \infty$, the inflection point T_{ip}, and other key points. From this perspective, the fundamental nature of the result was revealed after converting to a unified dimension for an ideal gas [3], based on the ideal gas equation of state $PV = nRT$. As a result, the universal gas constant R was canceled. The activation factor then took the following form:

$$P_a = \exp\left(-\frac{T_m}{T(1+n)}\right)$$

When analyzing this expression at $T = T_m$, it led to further simplification:

$$P_{a,m} = \exp\left(-\frac{1}{1+n}\right)$$

At $n = 0$ $P_{a,0} = e^{-1} = 37$ at $n \to \infty$ $P_{a,\infty} = 1$ and at $P_{a,m}=1-P_{a,0}=0{,}63$.

The transformations of the thermodynamic system, obtained based on the law of energy conservation, were found to be very close to the probability of system separation. In this approximation, it was more justified to adopt the standard model P_a (29).

The attempt to refine the activation factor demonstrated the adaptability of the probabilistic grinding model. It also showed that the model was open for further development. All influencing factors were considered. However, attention needed to be given to the necessity of eliminating the ambiguity surrounding the very meaning of activation energy.

The results of a single-point measurement of the size distribution of materials processed in the MShR 3.2 × 3.1 mill are presented in **Table 2**. In addition, a balance over the coarse size fractions was calculated, taking into account the aforementioned material streams: discharge, sands, and overflow. These data are given in **Table 3**. Overall, they may be considered sufficiently representative; however, certain features of the size distribution should be noted, likely arising from the single-point nature of the measurements as well as the specific operating characteristics of the spiral classifier.

Table 2 Particle size distribution of materials processed in the MShR 3.2 × 3.1 mill.

Fraction number, j	Size class, mm	Content, %			
		In ore	In discharge	In sands	In overflow
1	-25+16	10.3	0.6	1.6	–
2	-16+12	27.4	2.0	17.2	–
3	-12+8	17.6	3.5	32.8	0.4
4	-8+6	12.8	5.8	23.7	1.6
5	-6+2.6	12.0	11.1	10.2	10.2
6	-2.6+1.6	7.6	14.0	3.0	16.8
7	-1.6+0.21	5.7	23.0	3.9	25.6
8	-0.21+0.15	1.0	6.4	1.1	6.7
9	-0.15+0.10	0.2	3.3	0.5	3.5
10	-0.10+0.071	0.8	1.0	0.8	2.5
11	-0.071+0.043	0.4	6.0	0.4	4.9
12	-0.043	4.2	23.3	4.8	27.8
Σ	–	100.0	100.0	100.0	100.0

Table 3 Material balance for coarse size fractions in the mill discharge, classifier sands, and classifier overflow.

Fraction number, *j*	Size class, mm	MShR discharge		KSN sands		KSN overflow		Sands + overflow	
		%	t/h	%	t/h	%	t/h	t/h	%
1	-25+16	0.6	0.44	1.6	0.14	–	–	0.14	0.2
2	-16+12	2.0	1.48	17.2	1.55	–	–	1.55	2.1
3	-12+8	3.5	2.58	32.8	2.95	0.4	0.26	3.21	4.4
4	-8+6	5.8	4.28	23.7	2.13	1.6	1.04	3.17	4.3
5	-6+2.6	11.1	8.19	10.2	0.92	10.2	6.60	7.52	10.2
6	-2.6+1.6	14.0	10.32	3.0	0.27	16.8	10.88	11.15	15.1
7	-1.6	63.0	46.46	11.6	1.04	71.0	45.97	47.01	63.7
Σ	–	100.0	73.75	100.0	9.00	100.0	64.75	73.75	100.0

In particular, the sands, as well as the crushed ore, contain a noticeable proportion of the finest fraction (-0.043 mm), about 4-5%. This indicates the slimes-like nature of this fraction, which is formed even during crushing mainly due to particle abrasion, and also reflects incomplete classification in the KSN. Furthermore, in the mill discharge, as in the overflow, the dominant size class is the seventh fraction (−1.6 + 0.21 mm), with yields of 23.0% and 25.6%, respectively; the yields of the −1.6 mm class are also comparable, at 63.0% and 63.7% (**Table 3**). At the same time, the first three coarsest fractions in the discharge account for only 6.1%, and even less in the overflow (0.4%). Compared with their content in the feed ore (55.3%), this characterizes the operation of the mill at the first stage of grinding as being primarily directed toward the breakage of coarse fractions. This is further confirmed by the dominant presence of these fractions in the sands (51.6%).

The results obtained from the single-point measurement of the mill operating parameters were adapted to the probabilistic grinding model. First, it is necessary to determine the overall size distribution of the feed, consisting of a mixture of ore and sands. This distribution was calculated using the weighted-average content formula.

$$P_{j,mixture} = \frac{P_{j,ore} \cdot Qore + P_{j,sands} \cdot Q_{sands}}{Qore + Q_{sands}} \quad (31.)$$

or in the calculated (theoretical) case

$$P_{j,ore} = \frac{64.75P_{j,ore} + 9P_{j,sands}}{73.75}$$

This composition is taken as the initial one and, in model (2), is denoted as P_{0j} in fractional units. At the same time, each size class is represented by its mean particle size d_j in SI units (m), while the finest class ($-d_j$) is described using a steep decay function.

$$x_i = (1-x)x^i = P_{0i} = (1 - P_{-d_j})P^i_{-d_j}$$

in terms of its content P_{-dj}:

$$P_{0i} = \left(1 - P_{-d_j}\right) P^i_{-d_j} \quad (32.)$$

where i denotes the indices of the additional size fractions, starting from c $i = 1$. This is required for a detailed accounting of all size classes down to a negligibly small lower fraction, with a specified accuracy of 0.001 (fractional units, i.e., 0.1%), while ensuring that the sum of the contents of all classes equals unity (1.000). The results calculated using Equation (31) are presented in **Table 4**.

Table 4 Particle size distribution of the ore–sands mixture fed to the MShR mill.

j	Average particle size		P_{0j}	
	mm	m	%	i.e.
1	20.5	$2.05 \cdot 10^{-2}$	9.24	0.092
2	14.0	$1.40 \cdot 10^{-2}$	26.2	0.262
3	10.0	$1.00 \cdot 10^{-2}$	19.5	0.195
4	7.0	$7.00 \cdot 10^{-3}$	14.1	0.141
5	4.3	$4.3 \cdot 10^{-3}$	11.8	0.118
6	2.1	$2.10 \cdot 10^{-3}$	7.0	0.070
7	0.905	$9.05 \cdot 10^{-4}$	5.5	0.055
8	0.180	$1.80 \cdot 10^{-4}$	1.0	0.010
9	0.125	$1.25 \cdot 10^{-4}$	0.2	0.002
10	8.55	$8.55 \cdot 10^{-5}$	0.8	0.008
11	5.70	$5.70 \cdot 10^{-5}$	0.4	0.004
12	-0.043	$-4.3 \cdot 10^{-5}$	4.3	0.043
Σ	–	–	100.0	1.000

The finest class (−0.043 mm) should be represented in greater detail by additional fractions with successive halving of particle size, starting from the preceding class ($j = 1$ with $d_{11} = 5.70 \cdot 10^{-5}$ m) , each with its corresponding fractional content determined using Equation (32) by substituting $P_{-0.043} = 0.043$. With an accuracy of 0.001, it was sufficient to represent the finest class by two fractions: $j = 12$ with $d_{12} = 2.85 \cdot 10^{-5}$ m and $P_{012} = 0.041$, and $j = 13$ with $d_{13} = 1.43 \cdot 10^{-5}$ m and $P_{013} = 0.002$, which together give $P_{0j} = 0.043$.

Thus, for the application of the probabilistic grinding model (2), the required data on the initial size distribution are fully defined. The next step is to calculate the grinding rate constants for each size fraction, k_j using a formulation in which the activation factor is expressed in terms of ball size rather than ball mass.

$$k_j = \frac{8[(d_j/d_b) - (d_j/d_b)^2]\,\omega G_b G_p}{(1+2w\sqrt{2D/g})(G_b/\gamma_b + G_p/\gamma_p + G_w/\gamma_w)^2 \gamma_b \gamma_p} \exp\left(-\frac{E_a}{RT + 0.5 M_g D(\gamma_b/\gamma_p)(d_b/d_j)^3}\right) \quad (33.)$$

When the mill operates with a mixed ball charge, the grinding rate constants are calculated from the size and total mass of each ball fraction and then summed. According to the initial data, for a total ball mass of 37800 kg and the above-mentioned fraction contents, the mass of balls with $d_{b,1} = 0.10$ m is $G_{b,1} = 18\,144$ kg, with $d_{b,2} = 0.08$ m, $G_{b,2} = 6\,426$ kg, with $d_{b,3} = 0.06$ m, $G_{b,3} = 10584$ kg, with $d_{b,4}$ (pebbles) ~ 0.03 m, $G_{b,4} = 2646$ kg.

Each ball fraction interacts with the entire mass of the ore–particle mixture within the pulp; therefore, it is necessary to determine the total mass of the particulate material (ore and sands), G_p, and the mass of water, G_w, present in the mill and entering the grinding rate constant. These characteristics are not measured directly, but they can be estimated as follows.

The ball charge represents the coarsest, heaviest, and geometrically most regular assemblage, which, upon mill shutdown, forms a relatively dense packing. In this state, the pulp remains within the free interstitial voids of the packing and covers the top layer of balls up to the formation of a "pulp level." Knowing the bulk density of the ball charge, $\gamma_{b,bulk}$, and the true density of the balls γ_b, the volume of the void space can be determined and equated to the volume of the particulate material and water, i.e., the pulp:

$$V_{pulp} = V_p + V_w = \frac{G_b}{\gamma_{b,bulk}} - \frac{G_b}{\gamma_b} = \frac{37800}{4600} - \frac{37800}{7860} = 3.408 m^3 \quad (34.)$$

The solids content of the mixture of water and particles is the same at the mill and at its discharge under steady-state operating conditions. Therefore, knowing the mass fraction of water in the pulp (24.2%) and that of the corresponding particulate phase (75.8%), the volumes and masses of these components can be determined from the following balance relationships, expressed as a system of two equations with two unknowns:

$$V_{pulp} = \frac{G_p}{\gamma_p} + \frac{G_w}{\gamma_w} \quad (35.)$$

$$G_p/G_w = \frac{75.8}{24.2} = 3.132$$

$$G_w = \frac{V_{pulp}\gamma_p\gamma_w}{3.132\gamma_w + \gamma_p} = 1\,578\ kg$$

$$G_p = 3.132 G_w = 4\,942\ kg$$

Thus, all the quantities required to express the concentration factor in terms of G_b, G_p и G_w have been determined. At the same time, the residence time of the particulate material in the mill can be calculated based on the continuity equation.

$$\tau = G_w/(Q_{ore} + Q_{sands}) \quad (36.)$$

thus obtaining the value of the grinding duration

$$\tau = \frac{4942}{73750} = 6.701 \cdot 10^{-2} h = 4.021\ min = 24\ s$$

This parameter is required for substitution into the integral model (2) to calculate the particle size distribution of the material and to compare it with experimental data.

Subsequently, the partial grinding rate constants for each ball size $d_{b,i}$ can be calculated using Equation (33), taking into account the total mass of each ball fraction $G_{b,i}$:

$$k_{j,i} = \frac{8[(d_j/d_{b,i}) - (d_j/d_{b,i})^2]\omega G_{b,i} G_p}{(1+2\omega\sqrt{2D/g})(G_b/\gamma_b + G_p/\gamma_p + G_w/\gamma_w)^2 \gamma_b \gamma_p} \exp\left(-\frac{E_a}{RT + 0.5 M_g D(\gamma_b/\gamma_p)(d_{b,i}/d_i)^3}\right) \quad (37.)$$

As usual, the initial values of the parameters E_a and M are taken as their model values for quartz: E_a = 9 170 J/mol, M = 0.0601 kg/mol. The known constants g = 9.807 m/s^2 and R = 8.31441 J/(mol·K) are also used. The rotational speed in SI units is 18.2/60 = 0.303 s^{-1}, and the temperature is assumed to be 298 K. In the calculated case, Equation (37) takes the form:

$$k_{j,i} = 5.671 \cdot 10^{-6}\left[\left(d_j/d_{b,i}\right) - \left(d_j/d_{b,i}\right)^2\right] G_{b,i} \exp\left(-\frac{9170}{2478 + 2.574\left(d_{b,i}/d_j\right)^3}\right)$$

The calculation results are presented in **Table 5** for an expanded size-distribution basis in order to account for the possible formation of finer fractions than those present in the initial material.

Table 5 Partial and overall grinding rate constants for different size fractions of the particulate material and ball charge in the MShR mill.

j	d_j, m	$k_{j.i}$, s^{-1}, for $d_{b.i}$, m				$\Sigma k_{j.i} = k_j$, s^{-1}
		0.10	0.08	0.06	0.03	
1	$2.05\cdot10^{-2}$	$1.68\cdot10^{-2}$	$6.95\cdot10^{-3}$	$1.35\cdot10^{-2}$	$3.25\cdot10^{-3}$	$4.05\cdot10^{-2}$
2	$1.40\cdot10^{-2}$	$1.24\cdot10^{-2}$	$5.26\cdot10^{-3}$	$1.07\cdot10^{-2}$	$3.75\cdot10^{-3}$	$3.21\cdot10^{-2}$
3	$1.00\cdot10^{-2}$	$9.26\cdot10^{-3}$	$3.99\cdot10^{-3}$	$8.34\cdot10^{-3}$	$3.34\cdot10^{-3}$	$2.49\cdot10^{-2}$
4	$7.00\cdot10^{-3}$	$6.70\cdot10^{-3}$	$2.91\cdot10^{-3}$	$6.19\cdot10^{-3}$	$2.68\cdot10^{-3}$	$1.85\cdot10^{-2}$
5	$4.30\cdot10^{-3}$	$4.23\cdot10^{-3}$	$1.85\cdot10^{-3}$	$3.99\cdot10^{-3}$	$1.84\cdot10^{-3}$	$1.19\cdot10^{-2}$
6	$2.10\cdot10^{-3}$	$2.12\cdot10^{-3}$	$9.32\cdot10^{-4}$	$2.03\cdot10^{-3}$	$9.77\cdot10^{-4}$	$6.06\cdot10^{-3}$
7	$9.05\cdot10^{-4}$	$9.23\cdot10^{-4}$	$4.08\cdot10^{-4}$	$8.92\cdot10^{-4}$	$4.39\cdot10^{-4}$	$2.66\cdot10^{-3}$
8	$1.80\cdot10^{-4}$	$1.85\cdot10^{-4}$	$8.18\cdot10^{-5}$	$1.80\cdot10^{-4}$	$8.95\cdot10^{-5}$	$5.36\cdot10^{-4}$
9	$1.25\cdot10^{-4}$	$1.28\cdot10^{-4}$	$5.69\cdot10^{-5}$	$1.25\cdot10^{-4}$	$6.23\cdot10^{-5}$	$3.72\cdot10^{-4}$
10	$8.55\cdot10^{-5}$	$8.79\cdot10^{-5}$	$3.89\cdot10^{-5}$	$8.54\cdot10^{-5}$	$4.26\cdot10^{-5}$	$2.55\cdot10^{-4}$
11	$5.70\cdot10^{-5}$	$5.86\cdot10^{-5}$	$2.60\cdot10^{-5}$	$5.70\cdot10^{-5}$	$2.85\cdot10^{-5}$	$1.70\cdot10^{-4}$
12	$2.85\cdot10^{-5}$	$2.93\cdot10^{-5}$	$1.30\cdot10^{-5}$	$2.85\cdot10^{-5}$	$1.42\cdot10^{-5}$	$8.50\cdot10^{-5}$
13	$1.43\cdot10^{-5}$	$1.47\cdot10^{-5}$	$6.51\cdot10^{-6}$	$1.43\cdot10^{-5}$	$7.15\cdot10^{-6}$	$4.27\cdot10^{-5}$
14	$7.13\cdot10^{-6}$	$7.34\cdot10^{-6}$	$3.25\cdot10^{-6}$	$7.13\cdot10^{-6}$	$3.57\cdot10^{-6}$	$2.13\cdot10^{-5}$
15	$3.56\cdot10^{-6}$	$3.66\cdot10^{-6}$	$1.62\cdot10^{-6}$	$3.56\cdot10^{-6}$	$1.78\cdot10^{-6}$	$1.06\cdot10^{-5}$
16	$1.78\cdot10^{-6}$	$1.83\cdot10^{-6}$	$8.11\cdot10^{-7}$	$1.78\cdot10^{-6}$	$8.90\cdot10^{-7}$	$5.31\cdot10^{-6}$
17	$8.91\cdot10^{-7}$	$9.17\cdot10^{-7}$	$4.05\cdot10^{-7}$	$8.91\cdot10^{-7}$	$4.46\cdot10^{-7}$	$2.66\cdot10^{-6}$

The input data for calculating the fraction yields using the probabilistic model (2), along with the calculation results and experimental P_j values for a residence time of τ = 241 s, are given in **Table 6**.

Table 6 Partial and overall grinding rate constants for different size fractions of the particulate material and ball charge in the MShR mill.

j	Size class, mm	d_j, m	k_j, s^{-1}	P_{0j}, i.e.	P_j (2), i.e.	$P_{j(\text{discharge})}$, i.e.
1	-25+16	2.05	4.05	0.092	0	0.006
2	-16+12	1.40	3.21	0.262	0	0.020
3	-12+8	1.00	2.49	0.195	0.005	0.035
4	-8+6	7.00	1.85	0.141	0.035	0.058
5	-6+2.6	4.30	1.19	0.118	0.152	0.111
6	-2.6+1.6	2.10	6.06	0.070	0.340	0.140
7	-1.6+0.21	9.05	2.66	0.055	0.302	0.230
8	-0.21+0.15	1.80	5.36	0.010	0.103	0.064
9	-0.15+0.10	1.25	3.72	0.002	0.008	0.033
10	-0.10+0.071	8.55	2.55	0.008	0.008	0.010
11	-0.071+0.043	5.70	1.70	0.004	0.004	0.060
12	–	2.85	8.50	(0.041)	0.040	(0.179)
13	–	1.43	4.27	(0.002)	0.003	(0.042)
14	–	7.13	2.13	0	0	(0.010)
15	–	3.56	1.06	0	0	(0.002)
16	–	1.78	5.31	0	0	(0)
–	-0.043	–	–	0.043	0.043	0.233
Σ	–	–	–	1.000	1.000	1.000

Fig. 4 presents a direct comparison between the calculated results obtained using Eq. (6) and the experimental particle size distributions. The comparison demonstrates good qualitative agreement for both coarse and fine size fractions, with close correspondence in the regions of fraction formation and the separation of their maxima. This indicates a consistent (symbate) behavior between the calculated and experimental distributions.

This agreement is of considerable technological importance, as it provides a reliable basis for separating coarse and fine particle classes in classification equipment. At the same time, it is evident that the calculated model slightly overestimates the content of coarse fractions while correspondingly underestimating the amount of fine fractions. This discrepancy may be attributed to several factors.

The factors associated with the probabilistic model primarily stem from the use of simplified material characteristics. Specifically, the calculations were performed using the properties of quartz alone (E_a = 9170 J/mol and M = 0,0601 kg/mol), an assumed temperature of 298 K (whereas the actual pulp temperature may differ), an average grinding ball falling height of H = 0,5D, and a simplified representation of the feed material by an average particle size of approximately 30 mm.

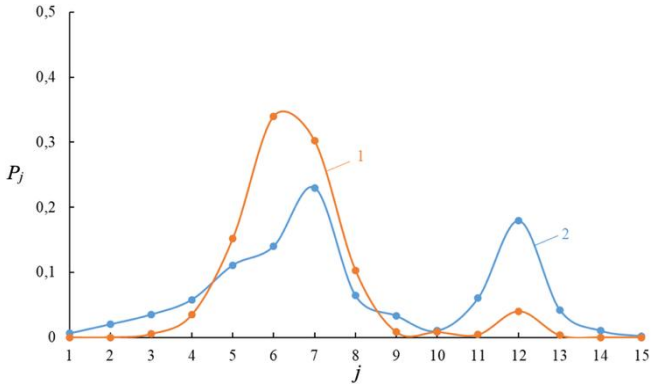


Fig. 4 Particle size distribution obtained from a single measurement of the discharge product from the grate ball mill (line 1, experimental data) and the distribution calculated using the probabilistic model of Eq. (6) (line 2).

From this standpoint, a single-point measurement of these parameters will inevitably contain random deviations from the predicted theoretical results. It is also essential to consider the possible deviation of the grinding process from a purely cascading regime toward an attrition-dominated regime, in which partial cascading of the material occurs during drum rotation without the ball–particle mixture falling into the impact zone.

Most likely, this explains the observed shift in the overall yield of coarse fractions toward finer ones, compared with the theoretically expected results. This is confirmed by calculations using the expression for the average rotational speed of the mill drum in the cascading regime.

$$\omega = 0.5762/\sqrt{D, s^{-1}}$$

Thus, for a drum diameter of the MShR 3.2 mill,

$$\omega = \frac{0.5762}{\sqrt{3.2}} = 0.322 s^{-1} = 19.3\ min^{-1}$$

The actual rotational speed of the mill is 18.2 rpm, i.e., lower than the average value, which may lead to a partial realization of the cascading (rolling) regime, accompanied by the formation of fine fractions due to the attrition of coarse particles.

Nevertheless, despite the inevitable influence of various sources of uncertainty that are difficult to account for within the probabilistic grinding model, the direct correlation between the calculated and experimental particle size distributions is characterized by a statistically significant correlation coefficient of R = 0.628. The corresponding Student's t-value is t_R = 3.9 which exceeds the critical value of 2 for the 95% confidence level, confirming the statistical significance of the correlation.

Therefore, the comparison between theoretical predictions and experimental particle size distributions can be used to adjust mill operating parameters as needed. Although the theoretical calculations may appear complex, they can be

readily implemented through computer programming and integrated into modern automated process control systems used in industrial operations.

Overall, it can be concluded that, despite the numerous disturbances encountered under industrial conditions, the probabilistic grinding model provides an adequate representation of the actual grinding process and can serve as a practical tool for controlling this highly complex operation.

Fig. 5 illustrates the evolution of the particle size distribution from the initial monofractional state to the formation and preservation of a log-normal distribution.

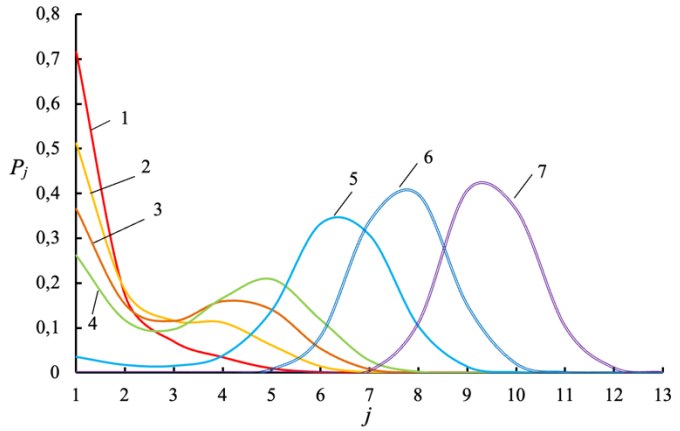


Fig. 5 Evolution of the particle size distribution (P_j, dimensionless) as a function of the size fraction index ($_j$) and grinding time: **1** – 60 s; **2** – 120 s; **3** – 180 s; **4** – 240 s; **5** – 600 s; **6** – 1200 s; **7** – 3600 s.

As shown in **Fig. 5**, the most pronounced changes in the particle size distribution occur during the first few minutes of grinding, consistent with industrial observations and highlighting the importance of maintaining optimal operating conditions through real-time process control.

The developed model may be useful not only for the operational adaptation of grinding conditions to the actual process, for example through the activation energy parameter, E_a, which reflects the intrinsic properties of the material and represents its overall resistance to crystal fracture. In principle, the proposed model can also be integrated into an automatic process control system for grinding operations to maximize the yield of target size fractions, particularly because the required calculations can be readily implemented in computational algorithms.

CONCLUSION

1. A physically grounded modification of the activation factor for probabilistic grinding models was developed by accounting for the combined contribution of potential and kinetic energy of grinding bodies in drum mills.
2. Analysis of the grinding media kinematics demonstrated that the effective ball fall height in cascading mode is approximately 0.83D instead of the conventionally assumed 0.5D. This resulted in a 17.6% increase in the estimated total mechanical energy transferred during grinding.
3. The proposed thermodynamically based approach for estimating activation energy using the material melting temperature eliminated the need for empirical fitting parameters while preserving the physical consistency of the model.
4. Model calculations for quartz grinding demonstrated high agreement between different formulations of the activation factor, with correlation coefficients of R = 0.973–0.996.
5. Industrial validation performed using an MShR 3.2 × 3.1 drum mill at the Zhezkazgan concentrator confirmed satisfactory agreement between calculated and experimental particle size distributions under industrial operating conditions (R = 0.628). The observed deviations were mainly associated with classifier instability, ore heterogeneity, and partial transition from cascading to attrition grinding mode.
6. The proposed model improves the physical interpretability and practical applicability of probabilistic grinding models and can be used for the analysis and optimization of industrial ore grinding processes.

Acknowledgements: This research is funded by the Committee of Industry of the Ministry of Industry and Construction of the Republic of Kazakhstan under program-targeted funding for scientific research for 2024-2026, BR23991563: «Creation of Innovative Resource-Saving Technologies for Mining and Integrated Processing of Mineral and Technogenic Raw Materials».

REFERENCES

1. G.S. Khodakov: *Physics of Grinding*; Nauka: Moscow, Russia, 1972.
2. E.W. Devis: Transactions of the American Institute of Mining and Metallurgical Engineers, 61, 1919, 250-296.
3. V.M. Avdokhin: *Fundamentals of Mineral Enrichment*, 2nd ed.; MSTU "Mining Book": Moscow, Russia, 2008, Vol. 2: *Technology of Mineral Enrichment*.
4. Z.A. Mikhaleva, D.A. Kopchev, V.P. Tarov: *Methods and Equipment for Processing Loose Materials and Solid Wastes*; TGTU: Tambov, Russia, 2002.
5. D. Foszcz, *et al.*: IOP Conference Series: Materials Science and Engineering, 427, 2018, 012031, https://doi.org/10.1088/1757-899X/427/1/012031
6. A.A. Abramov: *Processing, Enrichment, and Integrated Use of Solid Mineral Resources*, Moscow State Mining University: Moscow, Russia, 2004, Volume 2: Technology of Mineral Enrichment.
7. A.D. Lynch: *Crushing and Grinding Cycles: Modeling, Optimization, Design, and Control*, Nedra: Moscow, Russia, 1981.
8. L.F. Bilenko: *Laws of Grinding in Drum Mills*; Nedra: Moscow, Russia, 1984.
9. A.V. Arestova: *Theoretical Foundations of Automated Control. Automation of Ore Dressing Plants*, Ural State Mining University: Yekaterinburg, Russia, 2005.
10. S. Baigereyev, G. Guryanov, A. Suleimenov, B. Abdeyev: Applied Science, 15, 2025, 7713. https://doi.org/10.3390/app15147713
11. I.M. Oskembekov, G.L. Katkeeva: Obogashchenie Rud, 2014(5), 2014, 51–54.
12. J.V. Nava, A.L. Coello-Velázquez, J.M. Menéndez-Aguado: Metals, 11(1), 2021, 71. https://doi.org/10.3390/met11010071
13. S.E. El-Mofty, A.M. Elbendari, K.A. Abukhazel, A.A. El-Midani: Obogashchenie Rud, 2020(6), 2020, 21–25. https://doi.org/10.17580/or.2020.06.04
14. P.V. Malyarov, P.A. Kovalev, A.V. Bochkarev, A.M. Dolgov: Obogashchenie Rud, 2018(3), 2018, 3–8. https://doi.org/10.17580/or.2018.03.01
15. T.P.R. de Jong: Minerals Engineering, 191, 2023, 107950. https://doi.org/10.1016/j.mineng.2022.107950
16. O. Krauze, D. Buchczik, S. Budzan: Sensors, 21(2), 2021, 667. https://doi.org/10.3390/s21020667
17. I. Göktas, O. Altun, N.A. Toprak, D. Altun: Minerals Engineering, 198, 2023, 108090. https://doi.org/10.1016/j.mineng.2023.108090
18. I. Beloglazov, V. Plaschinsky: Materials 17, 2024, 795. https://doi.org/10.3390/ma17040795
19. Y.L. Liu, J.Y. Dai, X.Y. Chen, Y.S. Luo: Journal of Industrial and Management Optimization, 20(8), 2024, 2719–2739. https://doi.org/10.3934/jimo.2024023
20. S.W. Lu, S.Y. Huang: A mesoscale endpoint predictive model of ore grinding particle size. In: *Proc IEEE 17th Int Conf Industrial Informatics* (INDIN), 2019. p. 603–606. https://doi.org/10.1109/INDIN41052.2019.8972162
21. M. Serajuddin, S. Mukhopadhyay, A.R. Kacham: Transactions of the Indian Institute of Metals, 76(8), 2023, 2253–2261. https://doi.org/10.1007/s12666-023-02926-0
22. T. Santosh, et al.: Separation Science and Technology, 58(1), 2023, 149–163. https://doi.org/10.1080/01496395.2022.2075754
23. T. Santosh, et al.: Particulate Science and Technology, 39(6), 2021, 663–675. https://doi.org/10.1080/02726351.2020.1795016
24. U. Ulusoy, et al.: J Energy Storage. 97, 2024, 112814. https://doi.org/10.1016/j.est.2024.112814
25. G.S. Abdelhaffez, H.M. Ahmed, H.A. Saleem: Mining of Mineral Deposits, 17(2), 2023, 71–81. https://doi.org/10.33271/mining17.02.071
26. L.G. Gerasimova, Y.V. Kuzmich, E.S. Shchukina, N.A. Yakovleva: Inorganic Materials, 60(11), 2024, 1380–1390. https://doi.org/10.1134/S0020168525700025
27. B. Öksüzoğlu, M. Uçurum: Powder Technology, 291, 2016, 186–192. https://doi.org/10.1016/j.powtec.2015.12.027

28. V.P. Malyshev, A.M. Makasheva, D.A. Kaikenov, Y.S. Zubrina: *The Random Nature and Probabilistic Model of Material Grinding*; Nauchny Mir: Moscow, Russia, 2017.
29. V.P. Malyshev, A.M. Makasheva: Integrated Use of Mineral Raw Materials, 3, 2014, 60–65.
30. V.P. Malyshev, B.T. Abdrakhmanov, A.M. Nurmagambetova: *Flowability and Plasticity of Metals*; Nauchny Mir: Moscow, Russia, 2004.